Internal Report ITeSRE/CNR 272/2000

April 2000

STRAYLIGHT CONTAMINATION FROM INTERNAL SOLAR SYSTEM BODIES IN PLANCK LFI OBSERVATIONS

C. Burigana[1], P. Natoli[2], N. Vittorio[2],
N. Mandolesi[1] and M. Bersanelli[3]

[1]*Istituto TeSRE/CNR, via P. Gobetti 101, I-40129 Bologna, Italy*
[2]*Dipartimento di Fisica, Università di Roma "Tor Vergata", via della Ricerca Scientifica 1, I-00133, Roma, Italy*
[3]*Dipartimento di Fisica, Università di Milano, and IFC/CNR via Celoria 16, I-20133, Milano, Italy*

Internal Report ITeSRE/CNR 272/2000

April 2000

STRAYLIGHT CONTAMINATION FROM INTERNAL SOLAR SYSTEM BODIES IN PLANCK LFI OBSERVATIONS

C. Burigana[1], P. Natoli[2], N. Vittorio[2],
N. Mandolesi[1] and M. Bersanelli[3]

[1]*Istituto TeSRE/CNR, via P. Gobetti 101, I-40129 Bologna, Italy*
[2]*Dipartimento di Fisica, Università di Roma "Tor Vergata", via della Ricerca Scientifica 1, I-00133, Roma, Italy*
[3]*Dipartimento di Fisica, Università degli Studi di Milano, via Celoria, I-20131, Milano, Italy*

SUMMARY – The Planck optical design is aimed to reject the contamination from the brightest and extended internal Solar System bodies, namely the Sun, the Earth and the Moon. Nevertheless, according to the Planck detailed optical design and scanning strategy, these bodies could in principle give non negligible straylight signals, owing to the radiation entering the lowest antenna response regions, very far from the main beam and from the opposite side with respect to the main spillover. Through detailed simulations, we evaluate in this work the straylight contamination from the Sun, the Earth and the Moon. by considering a far antenna pattern as derived from recent accurate optical simulation codes. We find that the largest contamination derive from the Sun. It peaks at about 0.03μK (0.12μK) with peak to peak variations in the sky of about 0.002μK (0.12μK) in the case of a simple scanning strategy (a scanning strategy including spin axis precessions). This work is based on Planck LFI activities.

1 Introduction

The Planck Surveyor[1] is the ESA space mission devoted to the study of the Cosmic Microwave Background. Planck will have an impact on a number of scientific issues, such as the physics of the early universe, structure formation theory and cosmological parameters determination. In order to reach the claimed level of precision it is important to keep systematics under control. In this paper we will focus on the behavior of the Planck Low Frequency Instrument (LFI, Mandolesi et al. 1998) antenna patterns. For simplicity, we will restrict our analysis to the 30 GHz LFI channel but the method can be easily extended to other, higher frequency, channels.

[1]http://astro.estec.esa.nl/SA-general/Projects/Planck/

Each PLANCK feed sees the external planets under a very wide range of orientations with respect to the direction of its maximum directivity and therefore with very different antenna responses. Due to their small angular size and their brightness, these sources produce high signals only in the main beam and therefore can not produce significant straylight contamination. The PLANCK optical design is aimed to reject the contamination from the brightest and extended internal Solar System bodies, namely the Sun, the Earth and the Moon. For this reason, they are seen from each antenna very far from the main beam and from the opposite side with respect to the main spillover, i.e. at the lowest antenna response levels. Nevertheless, these bodies could in principle give non negligible straylight signals, according to the PLANCK detailed optical design and scanning strategy.

Through detailed simulations, we evaluate in this work the straylight contamination from internal Solar System objects, by considering a far antenna pattern as derived from recent accurate optical simulation codes.

The plan of this paper is as follows. In section 2 we describe our main tools and assumptions. In section 3 we present our results on straylight evaluation from the Sun, the Earth and the Moon. In section 4 we discuss these results and draw our main conclusions.

2 Simulation of PLANCK observations

The selected orbit for the PLANCK satellite is a Lissajous orbit around the Lagrangian point L2 of the Sun-Earth system (e.g. Bersanelli et al. 1996). The spacecraft spins at 1 r.p.m. and the field of view of LFI is around the telescope optical axis at a given angle α from the spin-axis direction, given by a unit vector, $\vec{s}$, choosen outward the Sun direction. In this work we consider a value of $\alpha = 80^\circ$, consistent with the available optical simulations (see section 2.1); values of α in the range between 80° and 90° are currently under study in the optimization of the scanning strategy. The spin axis will be kept parallel to Sun–spacecraft direction and repointed of $\simeq 2.5'$ every $\simeq$ hour. In addition, a precession of the spin-axis with a period, P, of $\simeq 6$ months at a given angle $\beta \sim 10^\circ$ about an axis, $\vec{f}$, parallel to the Sun–spacecraft direction (and outward the Sun) and shifted of $\simeq 2.5'$ every $\simeq$ hour, has been considered in this paper.

The code we have implemented for simulating PLANCK observations for a wide set of scanning strategies has described in detail in Burigana et al. (1997, 1998) and in Maino et al. (1999) where detailed informations are given, concerning the relevant reference frames, the convolution of the sky signal with the main beam pattern, the LFI receiver noise and the handling of the simulated data streams.

2.1 Coordinate systems and input antenna patterns

For the simple scanning strategies considered here, the directions of the spin axis (given by a unit vector $\vec{s}$, along the satellite spin axis outward the Sun direction) and of the telescope axis, z, (given by a unit vector $\vec{p}$) at each integration time are simple functions of given the epoch, the spinning frequency f_s and the angle α. On the plane tangent to the celestial sphere in the central direction of the field of view, i.e. on the field of view plane of the PLANCK telescope, we choose two coordinates x and y, with unit vector $\vec{u}$ and $\vec{v}$ respectively, according to the convention that the unit vector $\vec{u}$ points always toward $\vec{s}$ and that x, y, z is a standard cartesian frame, referred here as "telescope frame" [2]. In general, the beam centre

[2] We note that the "telescope frame" defined above may be or not equivalent to the "primary mirror frame" depending on the absence or presence of a tilt angle between the primary mirror axis and the central direction of the sky field of view. For example, a recent optical configuration studied by ESA exibits a tilt angle of $\simeq -3.75^\circ$.

will be identified by its unit vector $\vec{b}$ in the frame x, y, z or equivalently the coordinates, x_0, y_0, of its projection on the plane x, y or, more usually, by its corresponding standard polar coordinates, the colatitude θ_B and the longitude ϕ_B. The PLANCK High Frequency Instrument (HFI, Puget et al. 1998) feedhorns will be located in a circular box in the centre of the focal plane and the LFI feedhorns in a ring around the HFI box. Therefore the corresponding positions of LFI beams on the sky field of view are significantly off-axis. For a telescope with $\simeq 1.5$ m aperture the typical 100 GHz LFI beam is located at $\simeq 2.8^\circ$ from the optical axis, whereas the 30 GHz beams are at about $\simeq 5^\circ$ from it.

In order to adopt in our simulations a full sky antenna pattern shape at large angles from the beam centre consistent with a realistic pattern, we directly use the optical results computed by the ESA (de Maagt et al. 1998) for the "Carrier Configuration" for the PLANCK telescope including shields. We describe the antenna pattern response, J, at large angles from the beam centre by using two standard polar coordinates θ_{bf} (between 0° and 180°) and ϕ_{bf} (between 0° and 360°) referred to the "beam frame", i.e. corresponding to the standard cartesian "beam frame" x_{bf}, y_{bf}, z_{bf} which is obtained by the "telescope frame" x, y, z when the unit vector of the axis z is rotated by an angle θ_B on the plane defined by the unit vector of the axis z and the unit vector $\vec{b}$ up to reach $\vec{b}$ [3].

In Fig. 1 we show several cuts of the main beam pattern at constant azimuths ϕ_{bf} from 0° to 360° (from the bottom to the top). The main feature is the main spillover, at $\theta_{bf} \sim 90^\circ$ from the main beam, which shows a response of ≈ -60 dB with respect to the maximum response and extends for few tens of degrees in θ_{bf} and in ϕ_{bf} (around $\phi_{bf} = 0^\circ$, i.e. always quite close to the direction of the axis x in the "telescope frame"), but other relevant features with similar response level and angular extension are located at different angles θ_{bf} from the beam centre as ϕ_{bf} changes, in particular at few tens of degrees from the beam centre (see e.g. de Maagt et al. 1998 and Burigana et al. 2000 and references therein for a more detailed discussion on their relation with the optical configuration and the corresponding straylight contamination induced by the Galaxy emission). In spite of their relative very low appearance, the most critical pattern regions for what concerns the straylight from Solar System internal bodies is that about $(\theta_{bf}, \phi_{bf}) \sim (90^\circ, 180^\circ)$ (the "central" region of Fig. 1), where the pattern response drops approximately down to ~ -100 dB with respect to the maximum response (we will call this pattern region "antispillover" in what follows). Where the antenna pattern is extremely low, we expect a poor reconstruction of its shape.

It is then extremely important to be sure a priori that the straylight from Solar System internal bodies is not a threath.

2.2 Celestial mechanics and scanning strategy

For simple scanning strategies, with the spin axis kept always parallel to the Sun–spacecraft direction, the input parameters relevant for the sky scanning are the angle α between the spin axis and the telescope optical axis and the beam location on the plane x, y.

A precession motion of the satellite spin axis $\vec{s}$ has been considered with the aim to improve the receiver noise destriping efficiency and the sky coverage and to have the chance to reduce the angle, E, between the Earth–spacecraft direction and the spacecraft spin axis for the optimization of the data transmission. This kind of scanning strategy is described by three other relevant parameters: the period P of the precession motion, close to 6 months, i.e. the period of the PLANCK Lissajous orbit; the (semi) amplitude of the precession β, close

[3] Properly, the standard of "GRASP8" code for optical simulations is to provide the far pattern in terms of a "colatitude" angle θ'_{bf} (between -180° and 180°) from the "polar" axis parallel z_{bf} and an "azimuthal" angle ϕ'_{bf} (between 0° and 180°) related to θ_{bf} and ϕ_{bf} by: $\phi'_{bf} = \phi_{bf}$ if $\phi_{bf} \leq 180^\circ$ and $\phi'_{bf} = \phi_{bf} - 180^\circ$ if $\phi_{bf} > 180^\circ$; $\theta'_{bf} = \theta_{bf}$ if $\phi_{bf} \leq 180^\circ$ and $\theta'_{bf} = -\theta_{bf}$ if $\phi_{bf} > 180^\circ$.

to 10°; and the angle ξ_0 between the direction of the z ecliptic axis and the projection of $\vec{s}$ on the plane hortogonal to $\vec{f}$ at the injection of PLANCK in its Lissajous orbit. For example, at the PLANCK injection in the considered Lissajous orbit we find a well defined minimum of E, with a value of $\simeq 5°$, for $\xi_0 \simeq 280°$ (see Fig. 2). The clockwise or anticlockwise of the precession will be appropriately choosen.

By setting $\xi_0 \simeq 5°$, we find values of E during the mission just spreaded by few degrees about 5° (see Fig. 3). Although in principle different choices for ξ_0 are possible (a better choice could be for example to minimize the average of E during the mission), this indicates that only minor changes are introduced by different prescriptions on the values of E. For comparison, in the case of a simple scanning strategy, E is found to range between $\simeq 3.5$ and 15 deg (see Fig. 4).

Burigana et al. (1997) provide all the relevant geometrical trasformations in the case in which $\vec{f}$ lies on the ecliptic plane, which holds if we neglect the PLANCK Lissajous orbit about L2. We have here updated our code to include also the positions of the Solar System bodies and the Lissajous orbit of the spacecraft (Bersanelli et al. 1997). In the present computations, we arbitrarily fix the orientation of the PLANCK telescope line of sight at the beginning of each scan circle data stream close as much as possible to the positive z ecliptic axis and set its rotation clockwise seen by the positive direction of $\vec{s}$.

For each repointing of the spin axis we compute $\vec{s}$ and possibly $\vec{f}$. In the case of precessions we also choose ξ_0 according to a given prescription.
We considered here a slightly simplified version of the baseline scanning strategy, but accurate enough for the 30 GHz beams, which show a FWHM angular resolution of about $33'$ (see Mandolesi et al. 1998): spin-axis shifts of $5'$ every 2 hours and 2160 samplings per scan circle, i.e. approximately 3 samplings per FWHM.

The orientation of the relevant frames as the satellite moves is implemented in the code: at each choosen integration time we determine the orientations in the sky of the telescope frame and of the beam frame, necessary for appropriately computing the pattern response in each considered sky direction.

2.3 Solar System object emission

The measured antenna temperature of a Solar System object, $T_{A,obj}$, at a given time, t, can be written as (Bersanelli et al. 1997):

$$T_{A,obj}(t) = \frac{\int_{4\pi} T_{obj}(\hat{\gamma}, t)\ J(\hat{\gamma}, t)\ d\Omega}{\int_{4\pi} J(\hat{\gamma})\ d\Omega} \qquad (1)$$

where $T_{obj}(\hat{\gamma}, t)$ and $J(\hat{\gamma}, t)$ are respectively the frequency and time dependent intrinsic antenna temperature of the considered object and the response of antenna beam pattern along a sky direction identified by the unit vector $\hat{\gamma}$. In this notation, the explicite dependence on t in J means that we consider the antenna pattern in a given sky direction by taking into account the current orientations of the relevant coordinate systems, as discussed in sections 2.1 and 2.2. In the present computations we assume $T_{obj}(\hat{\gamma}, t)$ constant in time. The solid angle of the external planets as seen by PLANCK is very small compared to the beam size; analogously, the solid angle of the internal objects is again very small compared to the angular scale for which significant variations of the far pattern response occur. We can then approximate the above equation by:

$$T_{A,obj}(t) \simeq \frac{T_{obj}\pi(R/d)^2\ J(\hat{\gamma}_{obj}, t)}{\int_{4\pi} J(\hat{\gamma})\ d\Omega}\,, \qquad (2)$$

where $J(\hat{\gamma}_{obj}, t)$ is the response of antenna beam pattern toward the considered object, R is the object radius and d its distance from the spacecraft. The integrated simulated antenna

response for the present tests is $\simeq 1.058 \times 10^{-4}$. On the basis of the results discussed at the end of this paper it is clear that a simple local convolution on the object angular extent for the internal Solar System objects do not add any relevant information in this context.

In practice, we work here by using the polar coordinates θ_{bf} and ϕ_{bf}, according to the section 2.1.

The straylight contamination from internal objects is clearly proportional to their intrinsic temperature. We will consider here the effect introduced by the Earth, the Moon and the Sun, the only internal objects that could be a threath for straylight, due to their $(R/d)^2$ ratios and intrinsic temperatures. We compute the intrinsic antenna temperature of the Earth, the Moon and the Sun assuming blackbody emissions and by choosing for their thermodynamic temperatures the values: $T_{th,earth} = 300$ K, $T_{th,moon} = 250$ K and $T_{th,sun} = 6000$ K.

3 Straylight by Solar System internal bodies

We have applied the method described in the previous section to the computation of the straylight contamination from the Moon, the Earth and the Sun for three different scanning strategies. First of all, we perform a consistency test by simply assuming that the PLANCK surveyor is constantly located in L2, at a fixed distance from the Earth, and a simple scanning strategy with the satellite spin axis always along the antisolar direction. In the second case we introduce a realistic Lissajous orbit around L2 for the PLANCK surveyor by considering the same scanning strategy as above. Finally, we include also a precession motion of the satellite spin axis. For this analysis we assume $\alpha = 80°$, the value adopted in the optical computation by de Maagt et al. (1998).

In the following subsections we present our results in terms of maps of straylight contaminations derived by coadding the data streams computed as above for one year of observation; we work here on the sphere by using the HEALPix pixelisation by Górski et al. 1998 (note that, for the two first considered cases, the choice of α and the adopted beam location on the sky field of view imply that not the whole sky is observed, a small "hole" existing in each of the two ecliptic poles: in this region we arbitrarily set the map value equal to the minimum value obtained in the observed region, for graphic purposes).

3.1 Simple estimate: Planck located in L2 – *case* 0).

Fig. 5 shows our results in terms of antenna temperature for the three considered objects. Note that the map of straylight contamination from the Earth is flat, owing to the choice of costant distance between PLANCK in L2 and the Earth and the simple scanning strategy adopted here. The straylight map from the Sun is only slightly modulated according to the small variation of the distance between L2 and the Sun during the year. It introduces a signal variation in the map at a level of about the 10% of its maximum, or, in other words, when we subtract the average of this contamination, the relevant residual effect exibits a peak to peak signal difference at a level of 0.002 μK. The only interesting pattern is produced by the Moon. Note the roughly periodic pattern with the 12 relative maxima produced by the rotation of the Moon around the Earth, on a plane tilted with respect to the ecliptic plane. This implies that the Moon is seen under different directions by the antenna pattern and that the distance between PLANCK and the Moon is not constant even for these different relative maxima, so producing the variations of the corresponding signals. Summing up, the patterns shown in Fig. 5 are in agreement with simple geometrical considerations, so validating our simulation code.

These computations clearly show that the straylight effect from internal Solar System bodies is very small, peaking at about 0.001, 0.0014 and 0.03 μK and with variation in the

sky of about 0.001 and 0.002 μK respectively in the case of the Moon and the Sun, and null for the Earth.

In the next section we present results referring to more realistic observational assumptions. On the other hand, since the flatness of the pattern response around the "antispillover" we don't expect a very strong dependence of the straylight contamination on the details of the scanning strategy, although variations within a factor ≈ 10 of the maximum effect may be introduced by variations of the view angle of the considered object with respect the antenna pattern frame.

3.2 Effect of the Lissajous orbit – *case i*).

By including the effect of the satellite motion around L2 we expect a relevant modification of the straylight contamination map from the Moon and the Earth. This is confirmed by our numerical simulations. The Moon straylight pattern continues to exibit its typical maxima, but their magnitude and regularity is obviously modified by the satellite motion. The modification of the straylight contamination map is even more evident in the case of the Earth: obviously the satellite motion cancel the flatness of the pattern found in the previous section.

In spite of these modifications, the most relevant result is that this effect, although increased, still remains very small, peaking at about 0.003 and 0.01 μK with peak to peak variation in the sky of the same magnitude, respectively in the case of the Moon and the Earth.

The map of straylight contamination from the Sun is obviously essentially not modified by the satellite motion, owing to the large distance of the Sun compared to the Lissajous orbit size.

3.3 Effect of a satellite precession motion – *case ii*).

As described in section 2.2, the definition of the scanning strategy requires in this case the choice of angle ξ_0, which determines the values of the angle E during the mission, when the other mission parameters are set. Of course the detailed behaviour of E depends on the exact Lissajous orbit and scanning strategy; on the other hand the present results clearly shows the advantage of including a precession motion to minimize E (compare Fig.s 3 and 4). This may or not be a critical issue according its impact on the data trasmission, a relevant topic which deserves detailed works.

By including the effect of a satellite spin axis precession motion the coadded maps of the straylight contamination from the Moon and the Earth are further complicated, in particular at the ecliptic polar caps.

In spite of these modifications, this effect remains again very small, peaking at about 0.001 and 0.01 μK and with peak to peak variations in the sky of the same magnitude in the case of the Moon and the Earth, respectively.

The most critical modifications occur in the case of the straylight contamination from the Sun. The spin axis precession induces modification of the Sun view angle from the antenna frame and it produces a complicated straylight pattern which overwhelms the slight modulation induced by the variation of the Sun distance during the year. Under the adopted simulation conditions, we find also a significant increase, by a factor $\simeq 4$, of the maximum contamination that now peaks at $\simeq 0.12\mu$K with a similar value of the peak to peak differential contamination in the map. Again this effect is small, but it has to be considered with caution. In fact, as discussed in section 2.1, this straylight contamination is produced by the very low antenna response in the antispillover region, where an accurate antenna response evaluation is probably very difficult if not impossible. Therefore, antispillover antenna responses possibly higher than those considered here, may introduce a systematic contamination that, since the

complication of the pattern induced by the spin axis precession, may be very difficult to remove in the data analysis.

So far, we have identified two arguments, the first, related to the optimization of the angle between the Earth–spacecraft direction and the spacecraft spin axis direction, and the second, related to the oattern and the magnitude of the Sun straylight contamination, respectively in favour and against spin axis precessions.

4 Conclusions

We have implemented in our PLANCK observation simulation code (Burigana et al. 1997, 1998 and Maino et al. 1999) the computation of the positions the main Solar System bodies and of the spacecraft (Bersanelli et al. 1997) to quantify the impact of the internal Solar System bodies in the Planck LFI observations. Of course the Moon, the Earth and the Sun are the only internal bodies that may introduce appreciable straylight contamination. This kind of effect depends also on the effective scanning strategy. We studied a realistic Lissajous orbit around L2 for the PLANCK surveyor by considering *case i*) the simple scanning strategy with the spin axis always parallel to the Sun–spacecraft direction and *case ii*) a precession motion of the satellite spin axis like that discussed in section 2.2.

By coadding the data streams computed as above we produce nearly full sky maps of averaged straylight contaminations. We find that in any case this effect is very small.

For the scanning strategy *case i*) the Moon and the Earth straylight peaks respectively at about 0.003 and 0.01 μK, with peak to peak variation in the sky of the same magnitude. As expected, for one year mission, the Moon straylight map exibits twelve relative maxima (with different levels, according to the combined effect of Moon and PLANCK orbits) and the Earth straylight map shows a pattern related to the PLANCK orbit. The Sun straylight map is only slightly modulated according to the small variation of the distance between the spacecraft and the Sun during the mission. It introduces a contamination variation in the map at a level of about 10% of the maximum effect, or in other words when we subtract the average of this contamination, a peak to peak differential contamination at a level of $\simeq 0.002\mu$K.

For the scanning strategy *case ii*) the straylight peaks at about 0.001 and 0.01 μK, with peak to peak variations in the sky of the same order, in the case of the Moon and the Earth, respectively. The spin axis precession induces modifications of the Sun view angle from the antenna frame and produces a complicated straylight pattern which overwhelms the slight modulation induced by the variation of the Sun distance during the year. We find a significant increase, a factor $\simeq 4$, of the Sun maximum contamination that now peaks at $\simeq 0.12\mu$K, with peak to peak differential contamination of the same order.

Again this effect is still small, but it has to be considered with caution. In fact, as discussed in section 2.1, this straylight contamination is produced by the very low response antenna in the antispillover region, where an accurate antenna response measurement is probably very difficult.

Acknowledgements. It is a pleasure to thank C.R. Butler, D. Maino, F. Pasian and F. Villa for useful discussions on Planck design and performances. We gratefully acknowledge K.M. Górski and all the people involved in the realization of the tools of HEALPix pixelisation, employed in this work. We gratefully thank P. de Maagt and J. Tauber for having shortly provided us their optical simulation results.

References

[1] Bersanelli M. et al., 1996, ESA, COBRAS/SAMBA Report on the Phase A Study, D/SCI(96)3

[2] Bersanelli M. et al., 1997, A&AS, 121, 393

[3] Burigana C. et al., 1997, Int. Rep. TeSRE/CNR 198/1997

[4] Burigana C. et al., 1998, A&AS, 130, 551

[5] Burigana C. et al., 2000, Int. Rep. TeSRE/CNR 269/2000

[6] De Maagt P., Polegre A.M. & Crone G., 1998, PLANCK – Straylight Evaluation of the Carrier Configuration, Technical Report ESA, PT-TN-05967, 1/0

[7] Górski K.M., Hivon E. & Wandelt B.D., 1998, to appear in "Proceedings of the MPA/ESO Conference on Evolution of Large-Scale Structure: from Recombination to Garching", Banday A.J. et al. (Eds.), astro-ph/9812350

[8] Maino D. et al., 1999, A&AS, 140, 1

[9] Mandolesi N. et al., 1998, PLANCK Low Frequency Instrument, A Proposal Submitted to the ESA

[10] Puget, J.L. et al., 1998, High Frequency Instrument for the PLANCK Mission, A Proposal Submitted to the ESA

Figure 1: Cuts of full antenna pattern in dB for the carrier configuration: the lines refer to the antenna response for θ_{bf} between 0° and 180° and, from the bottom to the top, with ϕ_{bf} at steps of 30° from 0° to 360° (each cut is vertically shifted for graphic purposes to have the value at the point at $\theta_{bf} = 0°$ equal to the considered value of ϕ_{bf}).

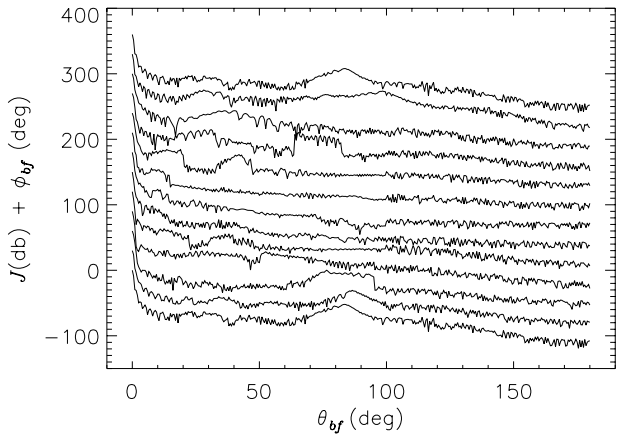

Figure 2: Angle between the spacecraft spin axis and the Earth-spacecraft direction at the injection in the Lissajous orbit as a function of the initial angle ξ_0.

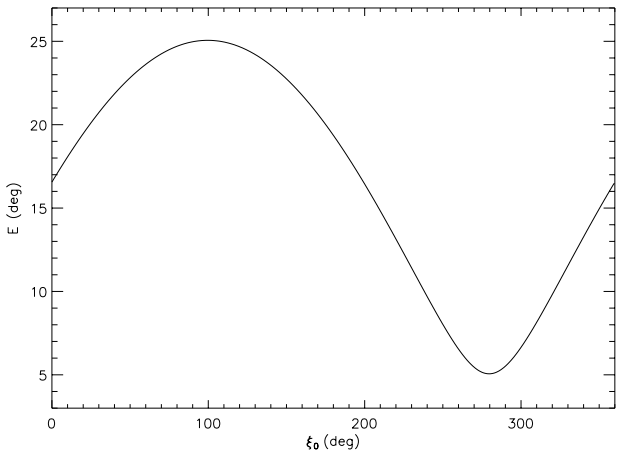

Figure 3: Angle between the spin axis and the Earth-spacecraft direction during the mission in the case of the scanning strategy with a spin axis precession motion.

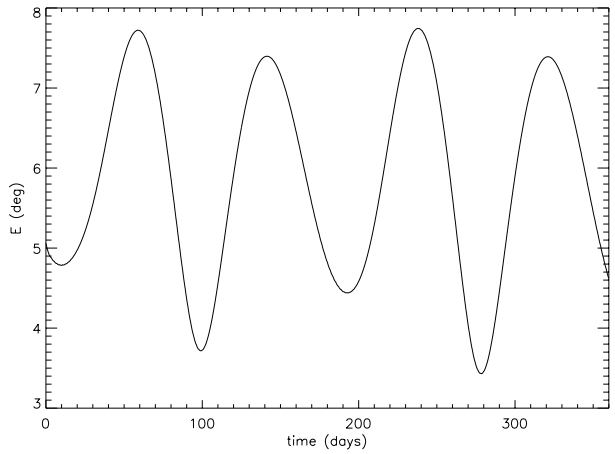

Figure 4: The same as in Fig. 3, but in the case of the scanning strategy with the spin axis always along the antisolar direction.

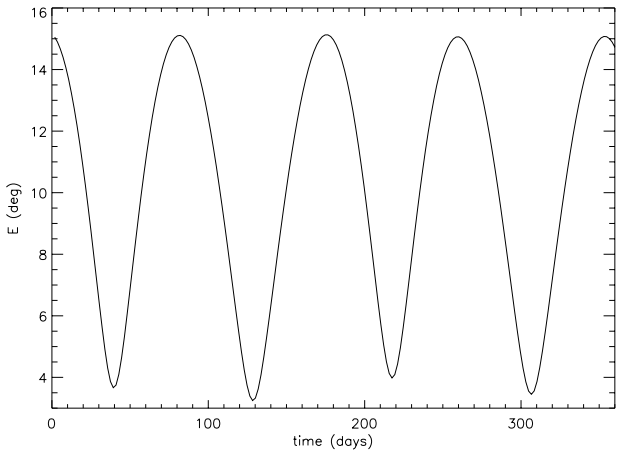

Figure 5: Map of coadded straylight contamination from the Moon, Earth and Sun in the case in which PLANCK is assumed to be located always in L2 and by considering the simple scanning strategy with the satellite spin axis always along the antisolar direction (antenna temperature expressed in μK).

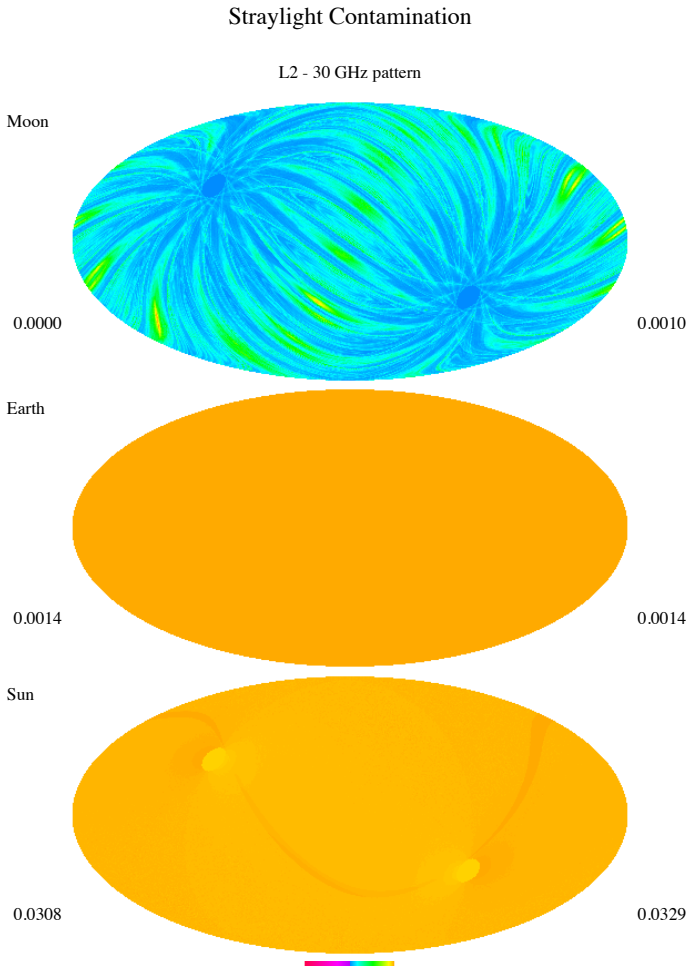

Figure 6: The same as in the Fig. 5, but including a Lissajous orbit of PLANCK around L2.

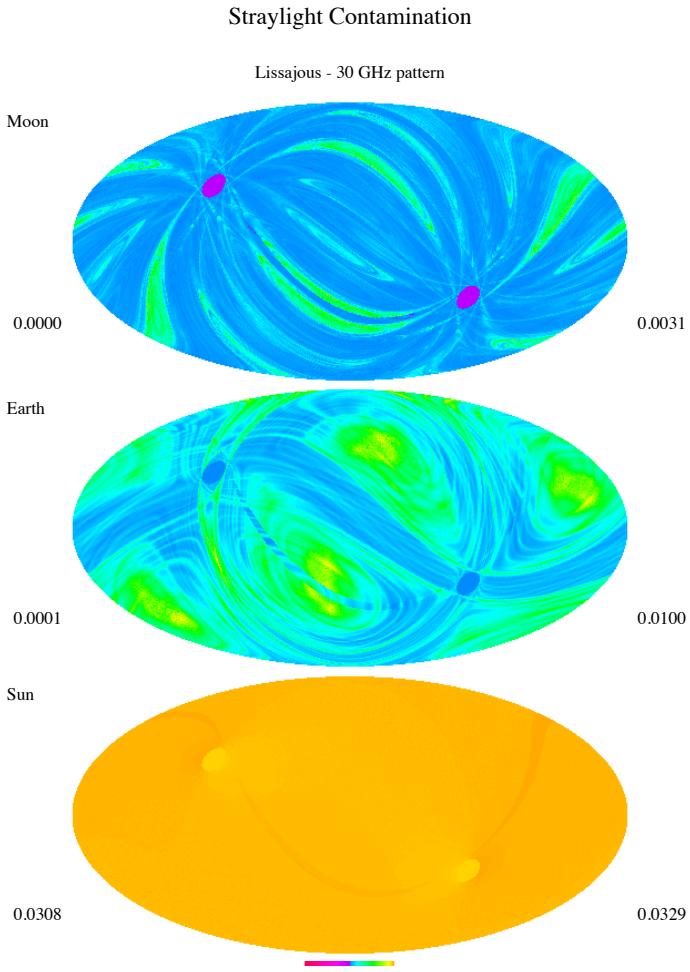

Figure 7: The same as in the Fig. 5, but including a Lissajuos orbit of PLANCK around L2 and a precession motion of the satellite spin axis.